Shear-wave splitting beneath the Snake River Plain suggests a mantle upwelling beneath eastern Nevada, USA[☆]

Kristoffer T. Walker[*], Götz H.R. Bokelmann[1], Simon L. Klemperer[2]

Department of Geophysics, Stanford University, Mitchell Building, Stanford, CA 94305, USA

Abstract

The Snake River Plain (SRP), a 90-km-wide topographic depression in southern Idaho, is a topographically anomalous feature in the western U.S. Previous seismic studies focused on the northeastern SRP to study its relationship with the Yellowstone hotspot. We present new teleseismic shear-wave splitting data from six broadband seismic stations deployed along the axis of the SRP from June 2000 to September 2001. We also analyze splitting at HLID, a permanent station of the National Seismic Network located ~ 100 km north of the plain. Splitting of individual teleseismic phases is consistent at all stations within 2σ errors, and we favor the interpretation of anisotropy with a single horizontal fast axis, although a dipping-axis interpretation is statistically permitted at two of the stations. Our station fast directions, as well as shear-wave splitting data from numerous other stations throughout the Basin and Range, are best explained by a lattice preferred orientation of olivine due to horizontal shear along the base of the plate associated with the gravitational spreading of buoyant plume-like upwelling material beneath eastern Nevada into a southwestward flowing asthenosphere (with respect to a fixed hotspot reference frame). This parabolic asthenospheric flow (PAF) model for the Great Basin is attractive because it explains the observed high elevations, high mantle buoyancy, low-velocity anomaly beneath eastern Nevada, high heat flow, and depleted geochemistry of some erupted basalts. The lack of Pliocene–Recent major volcanism in eastern Nevada suggests that a significant amount of the buoyancy flux is due to compositional buoyancy. Our splitting station delay times vary in a way not predicted by the PAF model, and can be explained by: a zone of aligned magma-filled lenses and/or partially molten dikes beneath the SRP lithosphere, a depleted olivine-rich residuum underneath the sides of the eastern SRP, and/or the effect of lateral lower crustal flow from beneath the eSRP toward its adjacent flanks.

---

1. Introduction

Extension and magmatism in the western U.S. have been studied for many decades. Prominent features that must be explained include the large volume of flood basalts that erupted ~17 Ma ago on the Columbia Plateau, high elevation, heat flow, development of north-striking normal faults and dikes in the Basin and Range, westward rotation of the southern Sierra Nevada, age progressions of volcanism origi-
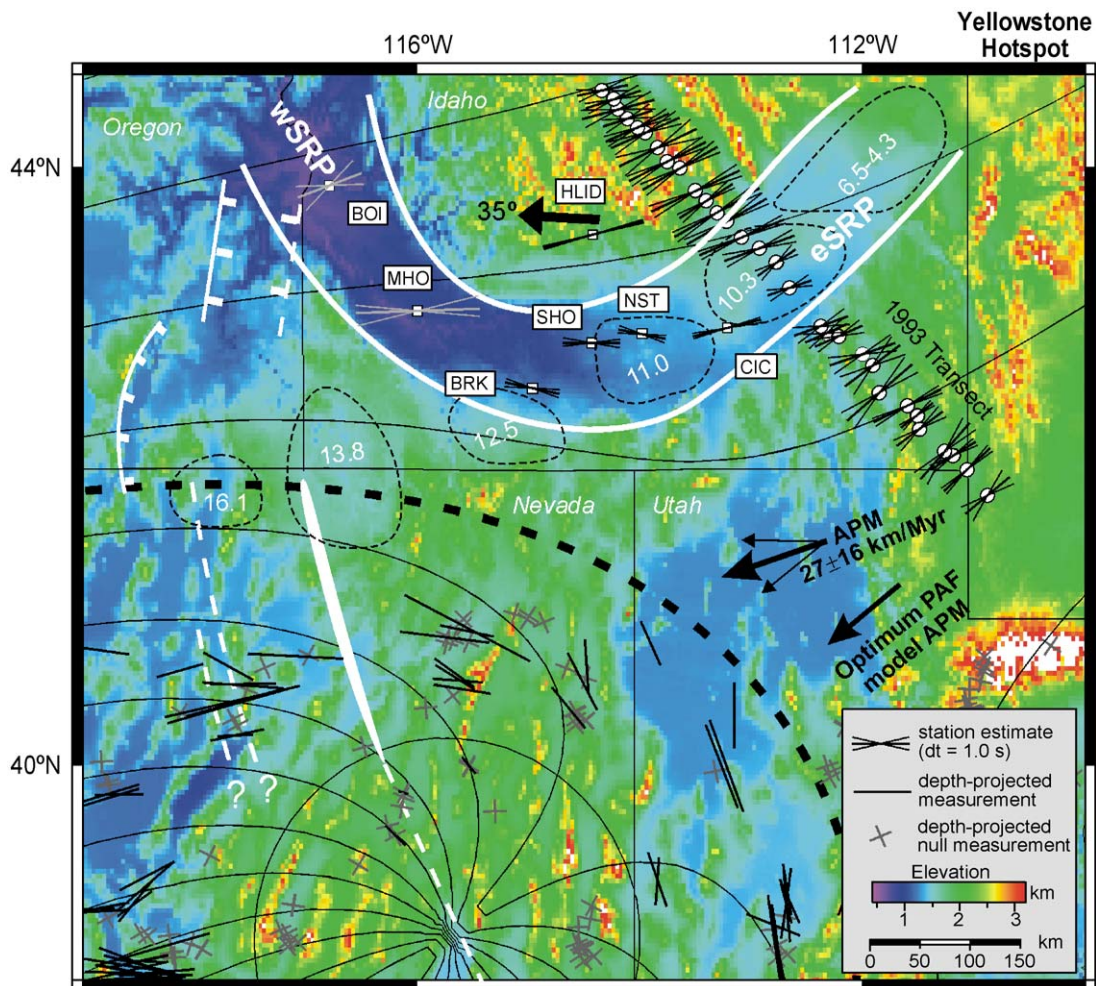

Fig. 1. Shear-wave splitting results in northern Nevada, Utah, and the Snake River Plain. White curves: Snake River Plain. Narrow black circles and enclosed numbers: age progression (in Ma) of silicic calderas defining Yellowstone hotspot track. Thick white line: northern Nevada rift dike swarm (dashed where inferred from aeromagnetic data). Squares: seismic stations analyzed in this paper. Circles: stations analyzed by Schutt et al. [33]. Black lines over the stations: station single-layer, horizontal fast-axis (HA) anisotropy models, parallel to the fast direction (ϕ) and with length proportional to delay time (dt). Thinner black lines: ϕ 2σ error bars. Gray estimates (MHO and BOI) are only based on one constrained measurement, and are not as reliable. Black lines not associated with stations: individual splitting measurements plotted above their 200-km piercing-point depth [50]. Null measurements: gray crosses oriented so that legs are parallel to the two possible fast directions. Dipping ϕ model for HLID: arrow in a lower hemisphere projection. Thin black curves: flow lines of the best-fitting PAF model [49]. Thick dashed curve: stagnation flow line separating plume material from normal asthenosphere. Note good agreement between most ϕ and PAF flow lines (see also Fig. 5), and concentration of null locations around the predicted plume center. Large circle: plume conduit, which is drawn only large enough to include the majority of null measurements. APM: absolute plate motion of North America (and 2σ uncertainties) from [19].

nating from northern Nevada and extending toward the Yellowstone and Newberry hotspots, and the topographically depressed Snake River Plain. Several geodynamic models have been proposed that explain some of these features including the arrival of a mantle plume head beneath the moving North American plate [1–5], gravitational collapse associated with a migrating triple junction and/or clockwise rotation of the Cascade–Klamath–Sierran blocks [6–10], and back-arc spreading [5,11,12].

One region of particular interest in understanding the western U.S. is the Snake River Plain (Fig. 1), a 90-km-wide, ~1000-m topographic depression in the southern half of Idaho that is divided into two separate branches. The western Snake River Plain (wSRP) runs from western Idaho at an elevation of 500 m toward the southeast for 300 km where it has an elevation of 1000 m. Here it bends around to connect with the eastern Snake River Plain (eSRP), which extends northeast 400 km to the Yellowstone hotspot at an elevation of ~2000 m. Geologic mapping and geochemical analysis show that 95% of the eSRP is covered by basaltic lava flows that occurred as fissure eruptions from volcanic rift zones and linear arrays of volcanic landforms and structures [13], which are probably the manifestation of dikes that intruded the crust perpendicular to the ENE/WSW least principal stress direction [14,15].

Beneath the basaltic lava flows of the eSRP lies a chain of rhyolitic tuff-filled calderas with an age progression from the ~16-Ma-old McDermitt volcanic field in northern Nevada to the Recent volcanism in the Yellowstone caldera in northwest Wyoming [13] (Fig. 1). The onset of wSRP extension appears to have accompanied moderate volcanism along the western rift 12–11 Ma ago, and continued with large volumes of basalt erupting ~9–7 Ma ago, and minor volcanism occurring since then [16]. Seismic and gravity data suggest that the middle crust beneath the northeastern eSRP is horizontally intruded by a tabular basaltic body of several kilometers thickness [17,18]. However, the existence of this body further to the southwest or in the wSRP has not been established, and therefore how the intrusion process, presumably related to Yellowstone hotspot magmatism, evolves with time remains unclear.

The age progression of volcanism and the rapid, voluminous eruption of the Columbia River basalts ~17 Ma ago are probably the most important observations in the interpretation that the eSRP is a hotspot track on the North American plate. This plate is moving westsouthwest at ~27 km/Ma [19] with respect to a fixed Yellowstone plume, the head of which impinged upon the lithosphere beneath northern Nevada ~17 Ma ago [20,21]. However, Geist and Richards [4] suggest that the hotspot may not have been "fixed". They show that the ~1000-m topographical depression of the wSRP may imply that it is not simply another graben that flanks the eSRP, but rather it could be a continuous hotspot feature that resulted from a deflection of the Yellowstone plume head by the subducting Farallon plate. Ebinger and Sleep [22] showed that horizontally spreading plume material could be guided along channels in the base of the lithosphere in zones of prior lithospheric thinning, which implies that the wSRP may have provided a channel for lateral plume flow if it was a zone of thinned lithosphere prior to (or developed during) the inception of the plume head. We analyze the splitting of teleseismic shear phases beneath four stations in the eSRP and two stations in the wSRP to help test between these hypotheses for the origin of the Snake River Plain, and more fundamentally, the other prominent features in the western U.S.

2. Deformation, anisotropy, and teleseismic shear-wave splitting

The mantle is primarily comprised of olivine, a seismically anisotropic mineral. When an aggregate of olivine grains is deformed via dislocation creep, a fabric or lattice-preferred orientation (LPO) develops where one or more of the three olivine crystallographic axes have a preferred orientation, leading to a bulk anisotropy for the aggregate. The orientation of the bulk anisotropy depends on which set of olivine dislocation slip planes are active in accommodating the deformation and what type of deformation is occurring [23–25]. For progressive simple shear, the fast [100] *a*-axes of olivine rotate toward the direction of shear. For uniaxial strain, the fast *a*-axes rotate away from the direction of shortening, and toward the direction of elongation. Therefore, the fast direction of the bulk anisotropy can be a proxy for mantle flow. A

bulk anisotropy can also develop due to a preferred orientation of structures such as cracks [26] or magma-filled lenses [27], and so some of the anisotropy could in principle have a non-mantle origin.

A teleseismic shear phase (plane wave) propagates through an anisotropic mantle as a pair of orthogonally polarized phases that travel at different speeds, the orientations of the polarization directions depending on the orientation of anisotropy with respect to the direction of wavefront propagation. The delay time that accumulates between these phases is proportional to the raypath length and magnitude of anisotropy sensed along the raypath.

3. Methodology

We use a modified version of the method of Silver and Chan [28] to make apparent splitting measurements. For each event, we band-pass filter the three-component waveforms between 0.02 and 0.2 Hz, and pick a master time window around the phase. Then for each event, we create 30 different time windows by randomly perturbing the master time window boundaries by up to $\pm 20\%$ of the length of the master time window. For each of these 30 windows, we either (1) assume the initial polarization direction (IPD) is equal to the back azimuth, and search over trial apparent fast direction (ϕ) and delay time (dt) for the optimum parameters that best remove the energy from the anisotropy-corrected transverse component of the core-refracted phases, or (2) calculate the IPD directly from the data, and search for the optimum parameters that maximizes the similarity between trial fast/slow waves for the S and ScS phases [28]. For each of the 30 analyses, the number of degrees of freedom is calculated directly from the windowed data. Then we stack the 30 misfit grids, find the global minimum, and derive the 95% confidence region from the average number of degrees of freedom. This is a similar procedure to that proposed by other workers [29,30] to calculate a constrained station splitting estimate from stacking misfit grids from different events. Through simple averaging, this grid-stacking modification increases the stability of the apparent-splitting analysis method and attenuates the affect of small time-window perturbations.

4. New splitting data

We analyze the splitting of teleseismic shear phases recorded by three-component CMG-40T sensors, which reliably detect signals down to periods of 30 s and are therefore suitable for teleseismic body-wave studies. During an IRIS PASSCAL experiment, we deployed four of these stations for one year (June 2000–July 2001) in the eastern Snake River Plain (eSRP), and deployed two in the western Snake River Plain (wSRP) for two months (July 2001–September 2001). The sensors were insulated from rapid temperature variations, and leveled on concrete slabs at the bottom of vaults 0.6–1 m deep. Only the eSRP stations recorded a high number of teleseismic waveforms. However, station SHO had operational problems, and only reliably recorded a fraction of the events recorded by the other eSRP stations. In addition, we also analyze waveforms recorded by HLID, a CMG-3 permanent broadband station of the National Seismic Network. Due to technical problems associated with collection and/or storage of HLID data, we were only able to analyze phases recorded at that station during 2002–2003, although some data prior to this time span exist and should become available in the near future [D. McNamara, personal communication, 2003]. In addition to our study, we also calculated teleseismic receiver-function stacks for these stations, and found evidence from PpPs phases (1) for along-axis crustal thickening (or equivalent average crustal velocity change) along the SRP from 40 km in the northeast to 42 km in the southwest, and (2) that a mid-crustal sill and possibly a partially molten lower crust thin to become undetectable toward the southwest [31].

We make measurements of apparent splitting of core-refracted phases (SKS, SKKS, PKS), core-reflected phases (ScS), and direct S phases on the Snake River Plain (SRP) stations. We analyze 34 phases (Supplement Table 1) recorded on at least one of the SRP stations, for a total of 60 phases analyzed: 34 SKS, 12 SKKS, 6 PKS, 6 S, and 2 ScS. For HLID, we analyze 12 phases: 8 SKS, 3 S, and 1 PKS. We are only interested in anisotropy beneath the seismic stations, and therefore reduce the possibility of source-side splitting by analyzing S and ScS events only from hypocenters deeper than 350 km. Fig. 2 shows examples of the apparent splitting measure-
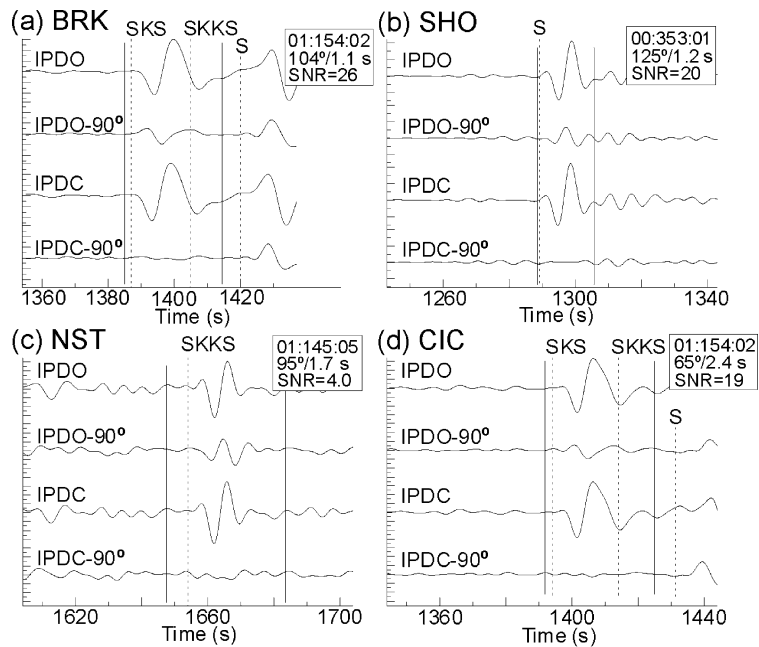
Fig. 2. Splitting examples for each station along the eastern Snake River Plain showing the horizontal-component waveforms parallel and perpendicular to the observed initial polarization direction (IPDO/IPDO-90°) and the corresponding anisotropy-corrected waveforms (IPDC/IPDC-90°). The boxes in the upper right indicate the date and UTC time of the analyzed event (year:julday:hour), the measured apparent fast direction and delay time, and the energy signal-to-noise ratio (SNR). Energy on the IPDO-90° component that is coherently out of phase with energy on the IPDO component is a diagnostic indicator of splitting. When applied to remove the phase difference, the splitting measurements successfully attenuate the energy on the IPDC-90° component.

ments for stations along the eSRP. There is a consistent fast direction rotation from WNW at BRK (a) to ENE at CIC (d).

The events recorded on the SRP stations (and HLID) have a fair distribution of back azimuths, and a good distribution of initial polarization directions (IPD), which are parallel to back azimuths (BAZ) for core-refracted phases. All analyzed phases have steeply dipping incidence angles INC = 5–28° at a depth of 200 km, and sample the upper mantle almost directly beneath the station, providing good lateral resolution. The coverage in BAZ, IPD, and INC is not ideal but is probably sufficient to discriminate between splitting from a single-layer model with a horizontal- or dipping-fast axis and a two-layer model with horizontal fast axes.

The apparent splitting measurements (ASMs) for each station are consistent with each other, and therefore a single fast direction (ϕ) and delay time (dt) can explain all the measurements within the 2σ errors (Supplement Table 2). We therefore use the

stacking method of Wolfe and Silver [30] to derive station splitting estimates (Supplement Table 3). For a two-layer anisotropy model beneath the station, a predictable variation of ASMs would exist with a 90° periodicity in IPD [32]. Station NST has the most variation in ASM versus IPD (Fig. 3). Simple averages of the NST splitting measurements are indicated by the horizontal lines. Note that although there is variation in the ASMs, the variation from the simple averages is generally not significant at a 95% confidence level. We performed grid searches for the optimum two-layer model parameters nonetheless (Supplement Table 3), and found that the misfit reduction for the best-fitting two-layer models was not significantly better than that provided by the simple averages.

Station SHO and HLID have ASMs that vary with back azimuth and incidence angle. Although the ASM measurements do not vary significantly away from the station estimates, they do vary in a manner that is predicted by a dipping fast-axis anisotropy model.

Fig. 4 shows the fit of the best dipping-axis model to the ASMs for station HLID. The dipping-axis models for both SHO and HLID are similar, with a fast axis pointing toward ~N80°W and dipping ~35°. However, the model for SHO is only constrained by three apparent splitting measurements, and the NW direction that is mostly responsible for this model has very large error bars. We therefore do not have enough reliable data at SHO to confirm a possible dipping-axis model. However, we can confirm that there is no evidence for a dipping-axis model at stations BRK, NST, and CIC (Supplement Table 3). Lastly for HLID, although the dipping-axis model explains 50% of the variation, we do not hold the dipping-axis model in high regard because the apparent splitting measurements themselves do not vary significantly away from the station estimate.

Fig. 4. Polar plot of apparent splitting measurements (black) versus back azimuth (angle) and incidence angle (radius) for ~200 km depth. There is a variation at station HLID (and SHO) that is better predicted with a single dipping fast-axis model (gray; oriented 280° and dipping 35°) than a single horizontal-axis or two-layer model.

Our preferred splitting models for the SRP and HLID splitting data are shown in Fig. 1. For the SRP stations, the preferred model is a single layer of anisotropy with a horizontal fast axis (station estimates). For HLID, we show both the horizontal- and dipping-axis models. There are interesting patterns observed in the data, e.g. the well-constrained clockwise rotation of station fast directions (ϕ) toward the southwest from ~N65°E (1993 transect) to ~N100°E (BRK). This rotation appears to follow the rotation of the axis of the Snake River Plain. However, further northwest along the wSRP, ϕ rotates back to ~N70°E, although these wSRP models are less well determined.

The delay times (dt) observed in the eSRP range from 0.8 to 1.2 s, and do not vary consistently along the axis. However, dt is much longer just to the north of the eSRP at stations HLID (1.8 ± 0.2 s) and MHO (2.2 ± 1.0 s). The estimate at MHO is based on one measurement with large error bars, and is not very reliable. On the Schutt et al. [33] transect, dt north of the eSRP are also almost twice as long as those on the eSRP.
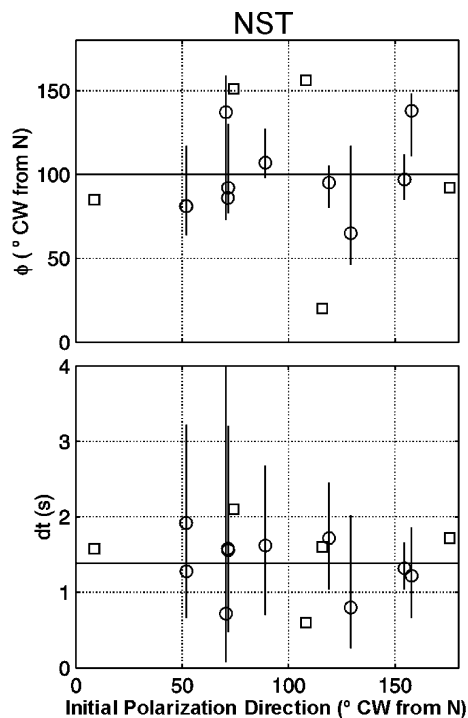

Fig. 3. Apparent splitting measurements versus initial polarization direction for station NST. Circles represent constrained splitting measurements (with 2σ error bars). Squares indicate null measurements (measurements of no significant splitting). There is no significant variation away from a simple average (horizontal lines), so a two-layer model is not required. The average above does not correspond exactly with the station average, which was derived via a different method.
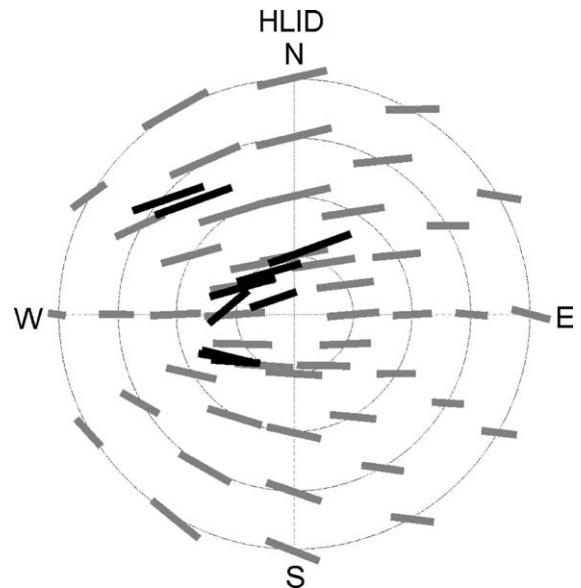
5. Discussion

There have been many hypotheses proposed to explain teleseismic shear-wave splitting. It is therefore important to determine which of these mechanisms is consistent with the data before deducing how they relate to the tectonic and geodynamic processes in the region.

The best method by which to determine uncertainties remains a subject of debate [34,35]. Our individual splitting uncertainties were estimated following the method of Silver and Chan [28], and our stacked station estimates following the technique proposed by Vinnik et al. [29] and Wolfe and Silver [30]. Alternative techniques based on a Bayesian formalism have been proposed [36]. We defer the discussion of uncertainty estimation to these respective papers, and in the following discussion we limit ourselves to hypotheses that fit our data within our 2σ uncertainties.

5.1. Fast directions

While the lithosphere beneath the SRP is ~ 40 km thick, the thickness along the flanks of the SRP is not as clear because of possible depleted olivine residuum in the asthenosphere beneath the flanks which has a higher-than average seismic velocity [37]. The SRP lithosphere has been highly modified by intrusion and, probably to a smaller extent, thinned by conductive erosion due to the recent passage of the Yellowstone hotspot. This lithosphere is probably characteristic of a volcanic continental rift (e.g. East African Rift), whereas the lithosphere along the flanks is more characteristic of young continental lithosphere. Fig. 5 shows the fast station estimates and 2σ errors (a) along the entire Snake River Plain from BOI to CIC, and (b) across the plain. We overlay predictions from the various mechanisms that might create anisotropy: fossilized anisotropy from past orogenic events (FOSS), recent lithospheric extension (EXT), magma-filled lenses and/or dikes (LENS), simple asthenospheric flow (SAF), channeled asthenospheric flow (CHAN), and parabolic asthenospheric flow (PAF).

Many mountain-building events have occurred in western North America throughout the Phanerozoic. Thrust faults from the Paleozoic and Mesozoic orogenies appear on both flanks of the eSRP, and strike
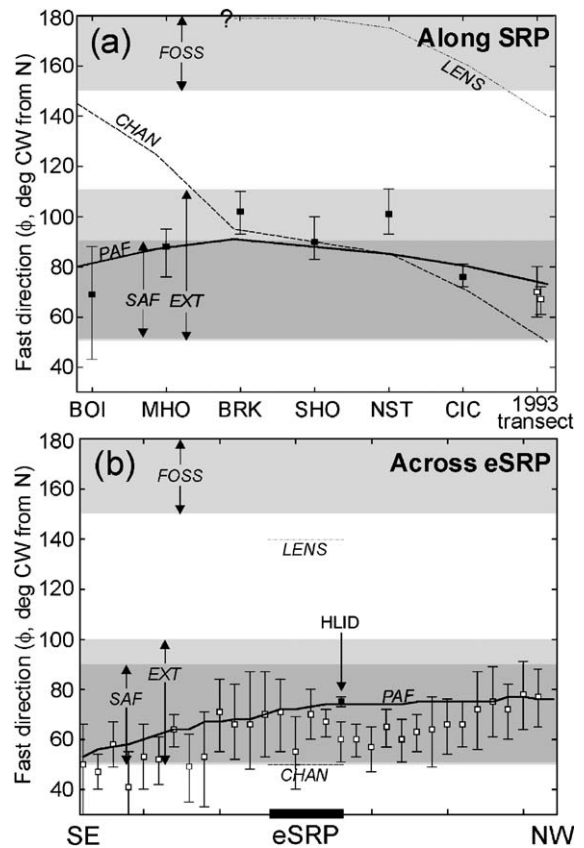

Fig. 5. Testing models of mantle anisotropy against fast splitting directions (ϕ) (a) along and (b) across the Snake River Plain (SRP). The "transect" station estimates in (a) and the station estimates in (b) (except for HLID) are from Schutt et al. [33]. The anisotropy models we test are fossilized anisotropy from past orogenic events (FOSS), recent extension (EXT), magma-filled lenses and/or dikes (LENS), simple asthenospheric flow (SAF), channeled asthenospheric flow (CHAN), and parabolic asthenospheric flow (PAF). SAF, EXT, and FOSS predict a range of ϕ (gray shaded regions). LENS, CHAN (dotted lines), and PAF (solid line—our preferred model) predict a specific orientation of ϕ at each station. The current extension direction is probably ENE–ESE throughout the SRP region. FOSS predicts a NNW–NNE ϕ. The LENS model requires the existence of partial melt, and may therefore only be important beneath the hotspot axis (b). The SAF prediction range is provided by the HS3-NUVEL1A [19] plate motion ($250 \pm 21°$). The CHAN model is confined to the plain, and does not extend beyond it in (b). The EXT model fits all the SRP data, but predicts much shorter delay times than that is observed. However, the PAF model similar to that of Savage and Sheehan [49] fits all the data in the SRP region as well as in Nevada and western Utah (Fig. 1).

NNW to the north, and NNW–NNE to the south [38]. The most recent orogenies were the Sevier and Laramide, both of which probably also resulted in east–west lithospheric shortening in the Snake River Plain region. Fast polarization directions (ϕ) in actively deforming mountain belts are usually perpendicular to the shortening direction [39]. Anisotropy can remain preserved or fossilized in the lithosphere for long periods of geologic time [28]. If FOSS is the dominant source of anisotropy beneath the Snake River Plain region, we would expect to find NNW–NNE ϕ (Fig. 5). However, observed ϕ throughout Idaho are clearly outside this range. Furthermore, although the lithospheric thickness beneath the flanks of the SRP is not well known, the mantle lithospheric thickness beneath the SRP is only ~ 10 km [37], which is not thick enough to give rise to $dt \sim 1.0$ s (this would require a thickness of at least 130 km).

Uniaxial extension of the lithospheric mantle via ductile thinning would produce an LPO of olivine fast *a*-axes in the direction of extension [24]. This hypothesis (EXT) has been used to explain splitting beneath the Red Sea rift, Baikal rift, Arctic ridge, and Rhine graben [39]. A shift in western U.S. deformation from roughly E–W compression to E–W extension occurred between 40 and 20 Ma ago during a shift from low-angle subduction to normal subduction [40–42]. In the northeast eSRP, Cenozoic extension appears to be ENE/WSW to the north, and WNW/ESE to the south of the eSRP [14]. The current extension direction in the southwest eSRP and wSRP is unclear at this time. Past extension in the wSRP region was E/W $\sim 15–12$ Ma ago as indicated by faulting, and NE/SW ~ 11 Ma ago as suggested by the orientation of a fissure system and the concurrently developing graben [16]. The geoid is higher above the northern eSRP flank than above the southern flank [43], and if the ENE/WSW geoid gradient in the wSRP is a predictor of the current extension direction, the region is probably extending ENE/WSW. The current Basin-and-Range extension direction in central Nevada (~ 600 km to the southwest) is oriented ESE/WNW [8]. Although the predictions are not well-defined because of the ambiguities mentioned above, the EXT hypothesis predicts ENE to ESE ϕ along the SRP, a range that brackets the observed ϕ (Fig. 5a). If this hypothesis is correct, then the ENE to E ϕ rotation from CIC to BRK and from BOI to BRK could be interpreted as a transition from

hotspot-dominated gravitationally driven extension to a more typical Basin-and-Range style of extension. However, the EXT model does not explain observed NNW–N ϕ in western Utah and northeast Nevada, or the region of nulls in eastern Nevada (Fig. 1). More importantly, as in the case against fossilized anisotropy as the dominant source of anisotropy, the lithospheric thickness beneath the SRP is not thick enough to result in $dt \sim 1.0$ s for the EXT hypothesis.

Vertically oriented magma-filled lenses can lead to a bulk anisotropy of the medium [27]. A preferred orientation of partially molten dikes could also lead to the same bulk anisotropy, although the magnitude may be smaller. Both of these mechanisms (LENS) could be produced in the presence of partial melt where there is a significant deviatoric stress in the lithosphere and/or asthenosphere in a normal-faulting stress state (σ_3 = horizontal, σ_1 = vertical [15]). The preferred orientation of these structures would strike parallel to σ_2, and consequently would lead to a bulk anisotropy with a fast direction parallel to σ_2. This mechanism has been used to explain ϕ that are subparallel to grabens in the Kenya Rift, Rio Grande Rift, and Baikal Rift Zone [44,45]. Stress-state indicators in the northeast eSRP suggest that σ_3 is ENE. The most recent eSRP volcanism was only ~ 2000 years ago [46]. There are many fissure and dike systems that cut across the eSRP that strike ca. perpendicular to the axis from CIC to at least SHO [13,47]. However, ϕ is $\sim 90°$ from that direction, and so it is clear that such a mechanism (LENS) is not the dominant cause of anisotropy.

The absolute plate motion direction and 2σ error for the North American plate where the eSRP stations were deployed is $250 \pm 21°$ [19]. If there is relative motion between the plate and underlying mantle, it is probably accommodated via simple shear in the lower lithosphere and asthenosphere. Such shear would induce a simple asthenospheric flow (SAF) in the direction of absolute plate motion (assuming a fixed underlying mantle), and could lead to an LPO of olivine fast *a*-axes and ϕ in the direction of plate motion if the strain occurs via dislocation creep [39]. This mechanism could explain ϕ on stations CIC, HLID, MHO, and BOI. However, because the plate-motion direction must remain consistent within the Snake River Plain region, the SAF model cannot explain all the station directions simultaneously.

Ebinger and Sleep [22] showed that the lateral flow of horizontally spreading plume material along channels in the base of the lithosphere could explain both the temporal and spatial distribution of uplift and volcanism throughout east and central Africa. For convenience, we use the word "plume" to refer to a roughly cylindrical, vertical conduit in the upper mantle with no specific depth of origin. Such lateral flow of plume material would lead to shear along the base of the plate, with fast olivine axes and ϕ parallel to the strike of the rift. This mechanism has been used to explain rift-parallel ϕ in the Rio Grande Rift [48]. The wSRP is generally thought to be a large graben, although its topography suggests a genetic relationship to the eSRP, which is identified by age dating to be the Yellowstone hotspot axis. Both the eSRP and wSRP probably have experienced lithospheric thinning, and have lithospheric channels developed beneath them. This mechanism explains the $\sim$ N65°E to $\sim$ N100°E ϕ rotation from the 1993 eSRP transect to station BRK, but not the rotation back to N70°E up the western Snake River Plain.

The SAF model does not explain significant variations in ϕ between stations. Savage and Sheehan [49] expand upon the SAF model to explain Basin-and-Range splitting by adding the effects of an upwelling to it, as has also been used to explain fast directions around the Hawaiian [34] and Eifel [K.T. Walker, G.H.R. Bokelmann, and S.L. Klemperer, "Shear-wave splitting around the Eifel hotspot: Evidence for plume-related flow", Geophys. J. Int., submitted for publication] hotspots. Savage and Sheehan proposed a parabolic asthenospheric flow (PAF) model to explain ϕ and null measurements in the Basin and Range by assuming that (1) ϕ are parallel (on average) to the flow lines, (2) there are no rapid changes in topography along the base of the lithosphere, and (3) null measurements occur directly above the upwelling (no splitting occurs along the conduit or in the lithosphere above it). The individual splitting measurements used in the Savage and Sheehan study and additional measurements from Savage [50] are also shown in Fig. 1. We calculate a similar PAF model using a slightly more easterly plume-center location at 38.8°N 115.7°W, their parabolic width ($\sim$ 290 km), and a slightly different plate-motion direction (230°) to match best the predictions to the data. The plate motion direction we use is within the 95% confidence region of the Gripp and Gordon [19] HS3-NUVEL1A plate motion direction ($250 \pm 21°$), and is parallel to the last 10 Ma of the Yellowstone hotspot trend. The stagnation streamline separates the plume material from "normal" asthenosphere, and is parallel to the fast directions in western Utah. We prefer this PAF model because it is the only model that simultaneously explains ϕ along the entire SRP (from CIC to BOI; Fig. 5a), across the eSRP [33] (Fig. 5b), and in western Utah and most of Nevada (Fig. 1).

5.2. Delay times

The average delay time (dt) on the eSRP ($\sim$ 1.0 s) is significantly shorter than along its flanks ($\sim$ 1.8 s), especially to the north and at MHO. The 2.2-s dt at MHO is not well constrained, but is still a useful observation given the lack of data from that region. The PAF model we present is purely kinematic, and does not predict variations in dt. However, for PAF, one would not expect significant variation in the magnitude of basal lithospheric shear over only tens of kilometers at great distances from the plume conduit. Therefore, we seek an additional mechanism to explain the shorter on-plain dt, and we present three possible mechanisms for this, noting that their summed effects could also explain the dt variation. First, the shorter dt could be due to the presence of parallel magma-filled lenses and/or partially molten dikes in the lithosphere. In the normal-faulting stress state of the eSRP, such structures would be vertically oriented and strike perpendicular to the least principal stress direction. To reduce the dt imparted by the PAF model, this hypothesis requires the structures to be oriented perpendicular to the fast direction imparted by PAF, i.e. from CIC to BRK, a ϕ rotation from $\sim$ N30°W to $\sim$ N (perpendicular to the eSRP axis). As mentioned above, such a rotation is approximately observed in the orientation of parallel fissures and dike systems along the eSRP.

This hypothesis can be quantified by calculating the partial melt necessary to explain both the low-velocity zone [37] and the observed decrease in dt beneath the eSRP. Assuming a lens density $\epsilon = 0.1$, an aspect ratio $\eta = 0.001$, and a melt P velocity of 1/3 the rock velocity, Kendall [27] calculated a maximum S anisotropy $\alpha = 11\%$. Crampin [26] calculated $\alpha = 11\%$ for water-

filled cracks, assuming the same ϵ and η as Kendall, but a crack P velocity 1/4 the rock velocity. Crampin also calculated the maximum α expected for various combinations of ϵ and η, where the P velocity of the rock and crack fluid was 5.8 and 1.5 km/s, and the S velocity (V_r) of the rock was 3.35 km/s. Faul et al. [51] found from controlled ultramafic rock-melting experiments that the majority of partial melt collects in penny-shaped lenses with η between 0.01 and 0.2. For $\eta < 0.2$ and $0.01 < \epsilon < 0.1$, the mean S velocity $V_m \approx 0.973 V_r$. In addition, for $\eta < 0.2$ a convenient empirical relationship exists: $\epsilon \approx \alpha$ [26]. Finally, the porosity $P = 4.21\eta\epsilon$. Extrapolating these results to the mantle, we assume a melt P velocity of $\sim 1/3$ the mantle velocity, $V_r = 3.4$ km/s, and $0.01 < \eta < 0.2$ [51]. We assume the ~ 100-km-thick low-velocity body beneath the eSRP [37] defines the thickness L of the partial melt region. Because the LENS model predicts fast directions perpendicular to those predicted by the PAF model, the anisotropy due to lenses would dilute that due to the PAF. Therefore we seek to explain ~ 0.8 s of splitting due to lenses. The equation for the delay time of shear-wave splitting is $dt = L(\alpha/V_m)$. Substituting in the above relations, we find $dt = (PL)/(4.10\eta V_r)$. To explain a 0.8-s dt dilution due to parallel lenses, we calculate a partial melt porosity $P = 1.15 \pm 1.05\%$.

The melt porosity can also be predicted (also with a large degree of uncertainty), directly from the tomographic data of Saltzer and Humphreys [37]. For an average $\eta = 0.05$, 1% partial melt porosity reduces V_p by 1.8% [51]. The region beneath the eSRP has a V_p reduction of 3–5%, and allows for a maximum partial melt porosity of 1.7–2.8%. However, temperature and composition also affect seismic velocities. A moderate excess temperature of 150 °C can explain a $\sim 1.0\%$ reduction in V_p [37], thereby reducing the partial melt porosity allowed by the tomography to 1.1–2.2%. As pointed out by Saltzer and Humphreys, the compositional variation may also lead to variations in V_p, and therefore affect the amount of partial melt required by the data to explain the dt reduction. Considering only the onset of melting of olivine, the iron-rich component melts first, and the depleted magnesium-rich (forsterite or Fo) residuum has a higher seismic velocity. A change in the solid–solution series from Fo_{88} to Fo_{92} (a 10% basaltic melt extraction) leads to a 1% increase in V_p [52], and would lower our melt porosity range to 0.6–1.7%. Therefore, our melt porosity calculated from the reduction in on-plain dt is consistent with the constraints placed on such porosity by tomography data alone with or without considering mild temperature or compositional affects. Our model predicts even shorter dt associated with NE fast directions in the northeast eSRP near the Yellowstone hotspot where we expect the partial melt porosity and extension rates to be higher.

A second hypothesis to explain the longer dt off the hotspot axis invokes compositional segregation via extraction of partial melt in the upwelling peridotite beneath the Yellowstone hotspot [37]. Depleted residuum is richer in anisotropic olivine than the zone of partial melt. This allows for the development of a stronger LPO in the residuum due to a lower concentration of pyroxene, which has a diluting or negative effect on the bulk anisotropy of peridotite [24]. If we assume that the upwelling peridotite has a 20% pyroxene component, and 10% is extracted via melt segregation, then the remaining peridotite residuum is comprised of about $\sim 90\%$ olivine. The zone of partial melt, which probably ponds to a certain extent at the base of the plate along the younger part of the hotspot axis, could have a much larger pyroxene concentration. Assuming (1) a linear relationship between pyroxene enrichment and decrease in dt (an over-simplification), (2) the zone of partial melt has a 50% olivine concentration (appropriate for basalt), (3) the zone of 90% olivine residuum accumulates along the flanks of the eSRP [37], and (4) the on-plain dt of 1.0 s is representative of 50% olivine composition, then the residuum would produce a dt of 1.6 s off the plain, which is close to the 1.8 s observed. Therefore, the shear strain induced by the PAF could lead to longer dt above such regions of pyroxene-depleted residuum.

Adding support to the second hypothesis, Saltzer and Humphreys [37] modeled the predicted topography expected for the crustal density structure [17,18,53] assuming isostasy. They found an anomalously high predicted elevation directly above the low-velocity anomaly (the northwest half of the eSRP). This high elevation can be reconciled with the observed lower elevation if there exists a dense mantle anomaly beneath the northwest side of the eSRP, which could be a zone of depleted residuum. Saltzer and Humphreys attribute the predicted elevations on and to the sides of the plain as due to variations in

crustal density not predicted by the crustal model, and instead argue for a larger compositional effect further out from the plain, especially in NW Wyoming.

A third hypothesis is that the on-plain *dt* could be reduced by lower crustal lateral flow away from the eSRP [54]. If the lower crust is decoupled from the upper crust and mantle, the gravitational potential energy provided by the regional high elevation would cause the lower crust to flow laterally out from beneath the eSRP. The addition of a dense mid-crust basaltic sill [17,55] would provide a local loading force that could enhance this flow considerably, leading to lower-crustal flow away from the eSRP and into the adjacent lower crust along both flanks. This would impart an LPO of olivine in the more viscous uppermost mantle with a NNW/SSE fast direction beneath the eSRP. The lower-crustal flow and resulting anisotropy would be less pronounced, non-existent, or in a different orientation beneath the flanks (to where the eSRP lower crust seeks to flow). A quantitative analysis is necessary to determine the magnitude of this effect on the uppermost mantle anisotropy. Observed azimuthal variations in P_n traveltime in the eSRP region (P_n travels within the first 10 km beneath the Moho) do not support this hypothesis, and instead indicate that the uppermost mantle beneath the eSRP has a N45°E fast direction [56]. However, this P_n result was of only fair quality, and represents a radial average over a ~650 km diameter, which would not reliably resolve anisotropy beneath the 90-km-wide eSRP.

6. Synthesis

Our shear-wave splitting observations are best explained by a single layer of anisotropy with a horizontal fast axis. The most robust feature of our splitting results is the rotation of the fast directions (ϕ) from ~N65°E at the 1993 eSRP transect to ~N100°E at BRK, and back to ~N70°E at BOI. Delay times (*dt*) along the axis do not vary, but are on average shorter than those off the axis (not including the poorly constrained *dt* for MHO). We explain these two features by a joint model: (1) a plume-like upwelling centered in eastern Nevada similar to that proposed by Savage and Sheehan [49], and (2) the presence of a preferred alignment of magma-filled

lenses [27,44] and/or partially molten dikes in the lithosphere of the SRP, the presence of depleted residuum rich in olivine beneath the northern flank of the eSRP [37], and/or the effect of lateral lower-crustal flow from beneath the eSRP toward its adjacent flanks.

The PAF model is consistent with and explains many other data. The circular region of nulls in eastern Nevada and ϕ throughout the northern Great Basin and across the eSRP (Figs. 1 and 5) are predicted by this model. The high Great Basin elevation, heat flow, and mantle buoyancy anomaly [15,57], low-velocity anomaly at 300 km depth [58,59], observed dynamic topography [60], and some petrological studies on Basin and Range basalts [61–64] also support this model.

The success of the eastern Nevada PAF model in explaining the splitting fast directions implies that anisotropy beneath the Snake River Plain is not controlled simply by drag associated with the overlying plate [33], nor a PAF model centered above the Yellowstone hotspot as one might expect for a Yellowstone plume. Instead, this model implies that there is a cylindrical mantle upwelling beneath eastern Nevada with a lateral flow pattern similar in scale to that calculated for the Hawaiian upwelling. Simple scaling to account for the difference in Pacific and North America plate speeds, 103 versus 27 km/Ma [19], suggests that the Nevada buoyancy flux is roughly 1/4 of the ~3 Mg/s beneath Hawaii [34,65] if all other factors are equal (asthenospheric thickness, conduit diameter, and rheology). This smaller buoyancy flux estimate of ~0.7 Mg/s suggests a smaller potential temperature. However, if the upwelling is due entirely to thermal buoyancy of mantle material, one would probably still expect to see minor volcanism beneath eastern Nevada given the region is in an area of continental extension, which facilitates magmatic intrusion. We speculate that a significant component of the buoyancy flux of the upwelling material beneath eastern Nevada is due to compositional buoyancy [66] such that the total buoyancy flux of ~0.7 Mg/s is consistent with the lack of Pliocene–Recent volcanism in central and eastern Nevada [67]. In addition, if this model is correct, the splitting data mostly originate from asthenospheric shear, and do not require a thick mechanical lithosphere in the western U.S. [68].

Because the Basin and Range province has been extending in the west and northwest direction for the last 30 Ma, and because the WSW absolute plate motion has been roughly stable for at least the last 17 Ma, it seems improbable that the currently observed plume-like upwelling provided the source of the Great Basin flood basalts ∼ 17 Ma ago. We speculate that the current upwelling is unrelated to the Yellowstone hotspot, and may in fact be a young upwelling that was being shielded by the Farallon plate until the slab window opened beneath eastern Nevada in the last several million years due to the northward migration of the Mendocino Triple Junction. This upwelling is not due to Basin and Range extension, which creates space to where passive upwelling material seeks to flow. Rather, this is an active upwelling unrelated to extension, since most of the upwelling material is spreading into the asthenosphere beneath plate, creating a parabolic pattern of mantle anisotropy via horizontal simple shear. Future high-resolution studies of the upper mantle velocity and anisotropy structure hold great promise for further exploring the relationship between Basin and Range tectonics and geodynamics.

Acknowledgements

References

[1] A.D. Brandon, G.G. Goles, A Miocene subcontinental plume in the Pacific Northwest; geochemical evidence, Earth Planet. Sci. Lett. 88 (1988) 273–283.

[2] D.S. Draper, Late Cenozoic bimodal magmatism in the northern Basin and Range province of southeastern Oregon, J. Volcanol. Geotherm. Res. 47 (1991) 299–328.

[3] K.L. Pierce, L.A. Morgan, The track of the Yellowstone Hot Spot, faulting, and uplift, in: P.K. Link, M.A. Kuntz, L.B. Platt (Eds.), Regional Geology of Eastern Idaho and Western Wyoming, Geological Society of America Memoir, vol. 179, 1992.

[4] D. Geist, M. Richards, Origin of the Columbia Plateau and Snake River plain: deflection of the Yellowstone plume, Geology 21 (1993) 789–792.

[5] M.L. Zoback, E.H. McKee, R.J. Blakely, G.A. Thompson, The northern Nevada Rift: regional tectono-magmatic relations and middle Miocene stress directions, Geol. Soc. Amer. Bull. 106 (1994) 371–382.

[6] J. Magill, A. Cox, Post-Oligocene tectonic rotation of the Oregon western Cascade Range and the Klamath Mountains, Geology 9 (1981) 127–131.

[7] J.J. Rytuba, D.B. Van der Meulen, Hot-spring precious-metal systems in the Lake Owyhee volcanic field, Oregon–Idaho, in: G. Raines, R.E. Lisle, R.W. Schafer, W.H. Wilkinson (Eds.), Geology and Ore Deposits of the Great Basin, Geological Society of Nevada Proceedings, 1994.

[8] W. Thatcher, G.R. Foulger, B.R. Julian, J. Svarc, E. Quilty, G.W. Bawden, Present-day deformation across the Basin and Range Province, western United States, Science 283 (1999) 1714–1718.

[9] P.J. Coney, T.A. Harms, Cordilleran metamorphic complexes; Cenozoic extensional relics of Mesozoic compression, Geology 12 (1984) 550–554.

[10] C.H. Jones, L.J. Sonder, J.R. Unruh, Lithospheric gravitational potential energy and past orogenesis: implications for conditions of initial Basin and Range and Laramide deformation, Geology 26 (1998) 639–642.

[11] G.P. Eaton, The Miocene Great Basin of western North America as an extended back-arc region, Tectonophysics 102 (1984) 275–295.

[12] W.K. Hart, J.L. Aronson, S.A. Mertzman, Areal distribution and age of low-K, high alumina olivine tholeiite magmatism in the northwestern Great Basin, Geol. Soc. Amer. Bull. 95 (1984) 185–195.

[13] M.A. Kuntz, H.R. Covington, L.J. Schorr, An overview of basaltic volcanism of the eastern Snake River Plain, in: P.K. Link, M.A. Kuntz, L.B. Platt (Eds.), Regional Geology of

Eastern Idaho and Western Wyoming, Geological Society of America Memoir, vol. 179, 1992.

[14] M.L. Zoback, M.L. Zoback, Tectonic stress field of the continental United States, in: L.C. Pakiser, W.D. Mooney (Eds.), Geophysical Framework of the Continental United States, Geological Society of America Memoir, vol. 172, 1989.

[15] T. Parsons, G. Thompson, R.P. Smith, More than one way to stretch: a tectonic model for extension along the plume track of the Yellowstone hotspot and adjacent Basin and Range Province, Tectonics 17 (1998) 221–234.

[16] B. Bonnichsen, M.M. Godchaux, Miocene to Pleistocene rhyolite–basalt volcanism and tectonism, western Snake River Plain and Owyhee Mountains, SW Idaho, abstract, Cordilleran Section, 98th Annual Meeting, May 13–15, 2002, Corvallis, Oregon, 2002.

[17] M.A. Sparlin, L.W. Braile, R.B. Smith, Crustal structure of eastern Snake River Plain from ray trace modeling of seismic refraction data, J. Geophys. Res. 87 (1982) 2619–2633.

[18] L.W. Braile, R.B. Smith, J. Ansorge, M.R. Baker, M.A. Sparlin, C. Prodehl, M.M. Schilly, J.H. Healy, S. Mueller, K.H. Olsen, The Yellowstone–Snake River Plain seismic profiling experiment: crustal structure of the eastern Snake River Plain, J. Geophys. Res. 87 (1982) 2597–2609.

[19] A.E. Gripp, R.G. Gordon, Young tracks of hotspots and current plate velocities, Geophys. J. Int. 150 (2002) 321–361.

[20] R.L. Christiansen, P.W. Lipman, Cenozoic volcanism and plate tectonic evolution of the western United States: II. Late Cenozoic, Philos. Trans. R. Soc. Lond., A 271 (1972) 249–284.

[21] R.L. Armstrong, W.P. Leeman, H.E. Malde, K–Ar dating, Quaternary and Neogene volcanic rocks of the Snake River Plain, Idaho, Am. J. Sci. 275 (1975) 225–251.

[22] C.J. Ebinger, N.H. Sleep, Cenozoic magmatism throughout east Africa resulting from impact of a single plume, Nature 395 (1998) 788–791.

[23] D. McKenzie, Finite deformation during fluid flow, Geophys. J. R. Astron. Soc. 99 (1979) 13655–13665.

[24] A. Nicolas, N.I. Christensen, Formation of anisotropy in upper mantle peridotites—a review, in: K. Fuchs, C. Froidevaux (Eds.), Composition, Structure and Dynamics of the Lithosphere–Asthenosphere System, Geodynamics Series, vol. 16, American Geophysical Union, Washington, DC, 1987, pp. 111–123.

[25] N. Ribe, On the relation between seismic anisotropy and finite strain, J. Geophys. Res. 97 (1992) 8737–8747.

[26] S. Crampin, Wave propagation through fluid-filled inclusions of various shapes: interpretation of extensive-dilatancy anisotropy, Geophys. J. Int. 104 (1991) 611–623.

[27] J.-M. Kendall, Teleseismic arrivals at a mid-ocean ridge: effects of mantle melt and anisotropy, Geophys. Res. Lett. 21 (1994) 301–304.

[28] P.G. Silver, W.W. Chan, Shear-wave splitting and subcontinental mantle deformation, J. Geophys. Res. 96 (1991) 16429–16454.

[29] L.P. Vinnik, V. Farra, B. Romanowicz, Azimuthal anisotropy in the Earth from observations of SKS at Geoscope and NARS broadband stations, Bull. Seismol. Soc. Am. 79 (1989) 1542–1558.

[30] C.J. Wolfe, P.G. Silver, Seismic anisotropy of oceanic upper mantle; shear-wave splitting methodologies and observations, J. Geophys. Res. 103 (1998) 749–771.

[31] K.T. Walker, Exploring Problems in Tectonics and Geodynamics with Seismology, PhD thesis, Stanford University, 2004.

[32] P.G. Silver, M.K. Savage, The interpretation of shear-wave splitting parameters in the presence of two anisotropic layers, Geophys. J. Int. 119 (1994) 949–963.

[33] D. Schutt, E.D. Humphreys, K. Dueker, Anisotropy of the Yellowstone Hot Spot wake, eastern Snake River Plain, Idaho, Pure Appl. Geophys. 151 (1998) 443–462.

[34] K.T. Walker, G.H.R. Bokelmann, S.L. Klemperer, Shear-wave splitting to test mantle deformation models around Hawaii, Geophys. Res. Lett. 28 (2001) 4319–4322 (2003, Reply to Comment by L.P. Vinnik, J.P. Montagner, N. Giradin, I. Dricker, and J. Saul, on "Shear-wave splitting to test mantle deformation models around Hawaii" by K.T. Walker, G.H.R. Bokelmann, and S.L. Klemperer, Geophys. Res. Lett, 28, 1676, doi: 10.1029/2002GL016712).

[35] L.P. Vinnik, J.P. Montagner, N. Giradin, I. Dricker, J. Saul, Comment on "Shear-wave splitting to test mantle deformation models around Hawaii" by Kristoffer T. Walker, Götz H.R. Bokelmann, and Simon L. Klemperer, Geophys. Res. Lett. 30 (2003) 1675 (doi: 10.1029/2002GL015751).

[36] I.G. Dricker, S.W. Roecker, L.P. Vinnik, E.A. Rogozhin, L.I. Makeyeva, Upper-mantle anisotropy beneath the Altai–Sayan region of central Asia, Phys. Earth Planet. Int. 131 (2002) 205–223.

[37] R.L. Saltzer, E.D. Humphreys, Upper mantle P wave velocity structure of the eastern Snake River Plain and its relationship to geodynamic models of the region, J. Geophys. Res. 102 (1997) 11829–11841.

[38] J.S. Oldow, A.W. Bally, H.G.A. Lallemant, W.P. Leeman, Phanerozoic evolution of the North American Cordillera; United States and Canada, in: A.W. Bally, A.R. Palmer (Eds.), The Geology of North America—An overview, Geological Society of America, Boulder, CO, 1989.

[39] L.P. Vinnik, L.I. Makeyeva, A. Milev, A.Yu. Usenko, Global patterns of azimuthal anisotropy and deformations in the continental mantle, Geophys. J. Int. 111 (1992) 433–447.

[40] G.P. Eaton, Regional geophysics, Cenozoic tectonics and geological resources of the Basin and Range province and adjoining regions, in: G.W. Newman, H.D. Goode (Eds.), Basin and Range Symposium, Rocky Mountain Association of Geologists, Denver, CO, 1979, pp. 11–39.

[41] M.L. Zoback, R.E. Anderson, G.A. Thompson, Cenozoic evolution of the state of stress and style of tectonism of the Basin and Range province of the western United States, R. Soc. Lond. Philos. Trans, A 300 (1981) 407–434.

[42] D.L. Harry, D.S. Sawyer, W.P. Leeman, The mechanics of continental extension in western North America: implications for the magmatic and structural evolution of the Great Basin, Earth Planet. Sci. Lett. 104 (1993) 398–416.

[43] D.A. Smith, D.R. Roman, GEOID99 and G99SSS: 1-arc-min-

ute geoid models for the United States, J. Geod. 75 (2001) 469–490.

[44] S. Gao, P.M. Davis, H. Liu, P.D. Slack, A.W. Rigor, Y.A. Zorin, V.V. Mordvinova, V.M. Kozhevnikov, N.A. Logatchev, SKS splitting beneath continental rift zones, J. Geophys. Res. 102 (1997) 22781–22797.

[45] A. Vauchez, G. Barruol, A. Nicolas, Comment on "SKS splitting beneath continental rift zones" by Gao et al., J. Geophys. Res. 104 (1999) 10787–10789; S.S. Gao, et al., Reply, J. Geophys. Res. 104 (1999) 10791–10794.

[46] A.W. Wood, J. Kienle, Volcanoes of North America: United States and Canada, Cambridge Univ. Press, 1990, 354 pp.

[47] D.R. Mabey, I. Zietz, G.P. Eaton, M.D. Kleinkopf, Regional magnetic patterns of the Cordillera in the western United States, Mem. Geol. Soc. Amer. 152 (1978) 93–106.

[48] E. Sandovol, J. Ni, S. Ozalaybey, J. Schlue, Shear-wave splitting in the Rio Grande Rift, Geophys. Res. Lett. 19 (1992) 2337–2340.

[49] M.K. Savage, A.F. Sheehan, Seismic anisotropy and mantle flow from the Great Basin to the Great Plains, western United States, J. Geophys. Res. 105 (2000) 13715–13734.

[50] M.K. Savage, Seismic anisotropy and mantle deformation in the western U.S. and southwestern Canada, Int. Geol. Rev. 44 (2002) 913–937.

[51] U.H. Faul, D.R. Toomey, H.S. Waff, Intergranular basaltic melt is distributed in thin, elongated inclusions, Geophys. Res. Lett. 21 (1994) 29–32.

[52] T.H. Jordan, Seismic velocities of garnet lherzolites and their geophysical implications, in: F.R. Boyd, H.O. Meyer (Eds.), The Mantle Sample: Inclusions in Kimberlites and other Volcanics, AGU, Washington, DC, 1979, pp. 1–14.

[53] X. Peng, E.D. Humphreys, Crustal velocity structure across the eastern Snake River Plain and the Yellowstone swell, J. Geophys. Res. 103 (1998) 7171–7186.

[54] M. Anders, N. Sleep, Magmatism and extension: the thermal and mechanical effects of the Yellowstone hotspot, J. Geophys. Res. 97 (1992) 15379–15393.

[55] C.S. Chiang, L.W. Braile, An example of two-dimensional synthetic seismogram modeling, Bull. Seismol. Soc. Am. 74 (1984) 509–519.

[56] G.P. Smith, G. Ekström, A Global Study of Pn Anisotropy, 1999.

[57] C.H. Jones, J.R. Unruh, L.J. Sonder, The role of gravitational potential energy in active deformation in the southwestern United States, Nature 381 (1996) 37–41.

[58] S. van der Lee, G. Nolet, Seismic image of the subducted trailing fragments of the Farallon plate, Nature 386 (1997) 266–269.

[59] S. van der Lee, G. Nolet, Upper mantle S velocity structure of North America, J. Geophys. Res. 102 (1997) 22815–22838.

[60] A.R. Lowry, N.M. Ribe, R.B. Smith, Dynamic elevation of the Cordillera, western United States, J. Geophys. Res. 105 (2000) 23371–23390.

[61] P.T. Leat, R.N. Thompson, M.A. Morrison, G.D. Hendry, A.P. Dickin, Compositionally diverse Miocene–Recent rift related magmatism in northwest Colorado: partial melting and mixing of mafic magmas from 3 different asthenospheric and lithospheric mantle sources, J. Petrol. (1988) 251–377 (Special Lithosphere Issue).

[62] R.N. Thompson, P.T. Leat, E. Humphreys, What is the influence of the Yellowstone mantle plume on Pliocene–Recent western USA magmatism? New Mexico Bur. Mines Miner. Resour., Bull. 131 (1989) 268.

[63] J.G. Fitton, D. James, W.P. Leeman, Basic magmatism associated with late Cenozoic extension in the western United States: compositional variations in space and time, J. Geophys. Res. 96 (1991) 13693–13712.

[64] M.F. Roden, N. Shimizu, Ion microprobe analyses bearing on the composition of the upper mantle beneath the Basin and Range and Colorado Plateau provinces, J. Geophys. Res. 98 (1993) 14091–14108.

[65] N. Ribe, U. Christensen, The dynamical origin of Hawaiian volcanism, Earth Planet. Sci. Lett. 171 (1999) 517–531.

[66] V.L. Hansen, Venus diapirs: thermal or compositional, Geol. Soc. Am. Bull. 115 (2003) 1040–1052.

[67] M.J. Cordery, G.F. Davies, I.H. Campbell, Genesis of flood basalts from eclogite-bearing mantle plumes, J. Geophys. Res. 102 (1997) 20179–20197.

[68] D. Schutt, E.D. Humphreys, Evidence for a deep asthenosphere beneath North America from western United States SKS splits, Geology 29 (2001) 291–294.

[69] P. Wessel, W.H.F. Smith, Free software helps map and display data, EOS Trans, AGU 72 (1991) 441.